

Inherited Berry curvature of phonons in Dirac materials with time-reversal symmetry

Sayandip Ghosh,^{1,*} Selçuk Parlak,² and Ion Garate^{2,†}

¹*Department of Physics, Visvesvaraya National Institute of Technology Nagpur, Nagpur 440010, India*

²*Département de physique, Institut quantique and Regroupement Québécois sur les Matériaux de Pointe, Université de Sherbrooke, Sherbrooke, Québec J1K 2R1, Canada*

(Dated: February 20, 2025)

The Berry curvature of phonons is an active subject of research in condensed matter physics. Here, we present a model in which phonons acquire a Berry curvature through their coupling to electrons in crystals with time-reversal symmetry. We illustrate this effect for BaMnSb₂, a quasi two-dimensional Dirac insulator, whose low-energy massive Dirac fermions generate a phonon Berry curvature that is proportional to the electronic valley Chern number.

I. INTRODUCTION

The Berry curvature of phonons in crystals has been introduced and extensively studied in the past decade, giving birth to the field of topological phononics [1–5]. Identifying and classifying materials with nontrivial phononic band geometry is a topic of ongoing interest [6–8]. One item that has received little attention thus far is the interplay between the phonon Berry curvature and the Berry curvatures of other quasiparticles of the crystal, notably electrons. Nevertheless, understanding this interplay could provide insights about the microscopic origin of the phonon Berry curvature.

From symmetry point of view, the phonon Berry curvature and the electronic Berry curvature are allowed in generic points of the Brillouin zone under the same circumstances, i.e. when space inversion (\mathcal{P}) or time-reversal (\mathcal{T}) symmetries are broken in the crystal; the product \mathcal{PT} must likewise be broken.

From microscopic point of view, however, there is no evident connection between the two curvatures. For instance, it is well-known that the electronic Berry curvature can be nonzero in the absence of phonons [9]. Conversely, models for topological phonons have been conceived, e.g. in two-dimensional honeycomb lattices [10], without any reference to electrons. Also, it has been reported that the phonon Berry curvature can be induced by a magnetic field in materials that have no electronic Berry curvature, like Si [11]. But, could there be more complex systems in which phonons would acquire a Berry curvature due solely to their coupling to topologically nontrivial electrons, or vice versa? This type of question has not been explored thus far.

Recently, Saparov *et al.* [12] have partially touched on the interplay between the phonon Berry curvature and the electronic band topology by investigating the electron-phonon interaction in the Haldane model. They have found that the molecular Berry curvature, which is an electronic Berry curvature resulting from ionic displacements, is proportional to the electronic Chern num-

ber (i.e. to the flux of the electronic Berry curvature through the Brillouin zone). This molecular Berry curvature modifies the equation of motion for lattice vibrations, ultimately resulting in a phonon Berry curvature that emerges from the electronic Chern number.

Crucially, the mechanism for the generation of the phonon Berry curvature in Refs. [11] and [12] relies on breaking \mathcal{T} either by magnetic order or by a magnetic field. Therefore, the question remains whether there could be a link between the phonon Berry curvature and the electronic Berry curvature in crystals that preserve \mathcal{T} . In the present study, we answer this question affirmatively.

To do so, we consider BaMnSb₂, a prototype quasi-two-dimensional Dirac insulator that breaks \mathcal{P} while preserving \mathcal{T} [13]. The dynamical matrix of this crystal, if described by a phenomenological force-constant model with two-body interactions, leads to phonons (which we call “bare” phonons) with a vanishing Berry curvature.

Upon inclusion of the coupling between lattice vibrations and the low-energy massive Dirac fermions of BaMnSb₂, a hybridization takes place between two linearly polarized, orthogonal bare phonon modes. This hybridization produces “dressed” phonons that are elliptically polarized [14], with an angular momentum that is proportional to the electronic valley Chern number (i.e. to the difference between two valley-projected Chern numbers). Because the direction of the angular momentum is locked to the wave vector, the dressed phonons have been characterized as “helical.” The helical texture of the phonon angular momentum in the Brillouin zone respects \mathcal{T} and crystal symmetries. As of now, there has been no experimental observation of this phonon helicity, though it could be accessible in the presence of temperature gradients [15, 16] or in Raman spectroscopy [17].

In the present work, we prove that the helical phonons in BaMnSb₂ possess a Berry curvature that is proportional to the electron-phonon coupling and to the electronic valley Chern number. Since the bare phonons had no Berry curvature, it is as though phonons “inherited” a Berry curvature from their coupling to topologically nontrivial electrons. This result is qualitatively different from that of Ref. [12] in that BaMnSb₂ preserves \mathcal{T} and the molecular Berry curvature is zero. The finding of

* sayandipghosh@phy.vnit.ac.in

† ion.garate@usherbrooke.ca

an “inherited” phonon Berry curvature in topologically nontrivial electron systems with \mathcal{T} symmetry is the main result from our work.

The rest of this work is organized as follows. In Secs. II and III we review the key electronic and lattice vibrational properties of BaMnSb₂. One insight from Sec. III is that bare, long-wavelength optical and acoustic phonons have a vanishing Berry curvature because the force constant model is symmetric under the exchange of cartesian coordinates. In Sec. IV, we consider the coupling between long-wavelength phonons and massive Dirac fermions. The effect of that coupling in the dynamical matrix and in the phonon Berry curvature is studied in Sec. V. It is found that the microscopic mechanism that produces phonon helicity is also responsible for the phonon Berry curvature. In Sec. VI, we consider the influence of a \mathcal{T} -breaking perturbation on the phonon Berry curvature. In a magnetic field, the “inherited” phonon Berry curvature is no longer an odd function of the phonon wave vector and therefore contributes to the thermal Hall effect. This contribution is proportional to the square of the phonon helicity and the electronic valley Chern number. Thus, thermal Hall effect can be regarded as an indirect probe of phonon helicity. Some technical details are collected in the appendices. Concerning units, $\hbar \equiv 1$ is adopted throughout the text.

II. PRELIMINARIES

We begin by briefly reviewing relevant aspects of BaMnSb₂, which we take here as a prototype Dirac material with time-reversal symmetry. It is a layered material with a quasi-two-dimensional (quasi-2D) electronic structure with low-energy bands being very weakly dispersive along (001) direction [13]. The xy crystal planes in which the Sb atoms are located form 2D rectangular lattices with two Sb atoms (Sb₁ and Sb₂) per unit cell. Distortion shifts Sb₂ atoms away from the center of the rectangles formed by Sb₁ atoms, resulting in a series of zigzag chains. Due to the zigzag distortion, the point group of BaMnSb₂ is C_{2v} , spanned by a two-fold rotation C_{2x} along the x -axis, a mirror plane $\sigma_v(xz)$ perpendicular to the y axis, and a mirror plane $\sigma_v(xy)$ perpendicular to the z axis.

The electronic band structure near the Fermi energy consists of two massive Dirac cones, related to one another by time-reversal symmetry, and situated at momenta (valleys) K_+ and K_- . These bands primarily come from the p_x and p_y orbitals of Sb atoms. The effective Hamiltonian [14] around a valley s is

$$\mathcal{H}_{\text{el}}^s = \sum_{\mathbf{k}} c_{s,\alpha,\mathbf{k}}^\dagger h_{\alpha\beta}^s(\mathbf{k}) c_{s,\beta,\mathbf{k}}, \quad (1)$$

where $\alpha, \beta \in \{p_x, p_y\}$ are orbital labels, c and c^\dagger are the electronic annihilation and creation operators, and $h_{\alpha\beta}^s$ is the matrix element of the $\mathbf{k} \cdot \mathbf{p}$ Hamiltonian

$$h^s(\mathbf{k}) = s [v_0(k_x \tau_x + k_y \tau_y) + m_0 \tau_z]. \quad (2)$$

Here, v_0 is the Dirac velocity, m_0 is the Dirac mass induced by the zig-zag distortion, and $\tau_{0,x,y,z}$ are Pauli matrices for the orbital index. Within this low-energy subspace, $\sigma_v(xy)$ corresponds to an identity matrix and does not change the 2D momentum. Thus, we only consider C_{2x} and time-reversal (\mathcal{T}) operations henceforth. The Hamiltonian transforms as $C_{2x} h_e^s(k_x, k_y) C_{2x}^{-1} = h_e^{-s}(k_x, -k_y)$ and $\mathcal{T} h^s(\mathbf{k}) \mathcal{T}^{-1} = h^{-s}(-\mathbf{k})$, where the symmetry representations are $C_{2x} = \tau_z$ and $\mathcal{T} = \tau_0 \mathcal{K}$ (\mathcal{K} stands for complex conjugation). Within one valley, we only have the combined symmetry $C_{2x} \mathcal{T} = \tau_z \mathcal{K}$.

III. BARE IN-PLANE PHONONS

In this section we calculate the Berry curvature of lattice vibrations involving the in-plane displacements of Sb ions. By “bare”, we mean phonons that are not coupled to low-energy Dirac fermions. We model those phonons via phenomenological short-range interatomic force constants that are symmetric under the interchange of cartesian coordinates. The coupling to Dirac fermions will be incorporated in Secs. IV and V, upon which the phonons will be called “dressed”.

A. Dynamical matrix

The crystal structure of a Sb layer in the xy plane is illustrated in Fig. 1, with $\delta a/2$ the atom displacement due to the zig-zag distortion of the lattice (the distance between the white and the black dots in units of the lattice constant). Owing to the two Sb atoms in the 2D unit cell, there exist six phonon modes (three acoustic and three optical) associated with vibrations of Sb atoms. These modes are characterized by the displacements of the two atoms away from their equilibrium positions, $(u_{1x}, u_{1y}, u_{1z}, u_{2x}, u_{2y}, u_{2z})$. In this work, we disregard the phonon modes with vibrations along the z -axis, since they are odd under mirror reflection $\sigma_v(xy)$ and therefore cannot couple to electronic states near Fermi level, which are even under $\sigma_v(xy)$.

Following Ref. [14], the bare in-plane lattice vibrations are *defined* through phenomenological force constants

$$\Phi_{\alpha\beta}(l\kappa, l'\kappa') = \gamma(l\kappa, l'\kappa') \hat{\mathbf{e}}_\alpha \hat{\mathbf{e}}_\beta, \quad (3)$$

where $(l\kappa)$ labels an atom κ in unit cell l , $\alpha, \beta \in \{x, y\}$, $\hat{\mathbf{e}}$ is the unit vector in the direction of the vector connecting atoms $(l\kappa)$ and $(l'\kappa')$, and $\gamma(l\kappa, l'\kappa')$ is the spring constant between atoms $(l\kappa)$ and $(l'\kappa')$. Using the atom labels of Fig. 1, the spring constants involving atom 0 are named as

$$\begin{aligned} \gamma_0 & \text{ (between atom 0 and atoms 1, 2, 3, 4)} \\ \gamma_1 & \text{ (between atom 0 and atoms 7, 8)} \\ \gamma_2 & \text{ (between atom 0 and atoms 5, 6).} \end{aligned} \quad (4)$$

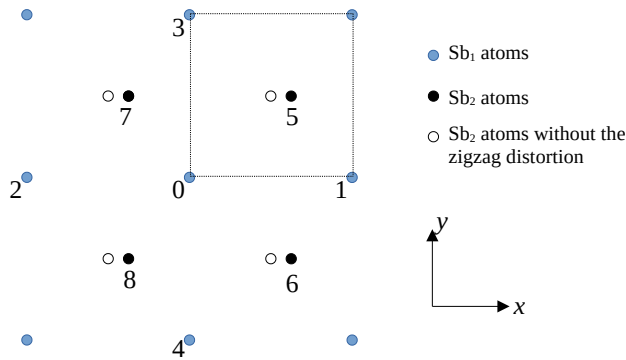


FIG. 1. Layer of Sb atoms in BaMnSb₂. The rectangular unit cell, of dimensions $a \times b$, is shown by the dotted lines. For simplicity, we take $a = b$ in the main text. This simplification does not result in qualitative changes to our main results.

The spring constants involving an atom different from 0 can be constructed similarly. The couplings between further neighbors are neglected.

We have also tried more general models for the bare force constants (cf. App. A), verifying that they do not bring about qualitative changes to the main results of our paper. One key property of these phenomenological models is that

$$\Phi_{\alpha\beta}(l\kappa, l'\kappa') = \Phi_{\beta\alpha}(l\kappa, l'\kappa'), \quad (5)$$

which, although known to hold for two-body forces [18], is more restrictive than the always-true condition $\Phi_{\alpha\beta}(l\kappa, l'\kappa') = \Phi_{\beta\alpha}(l'\kappa', l\kappa)$ [19].

The bare phonon polarizations and frequencies are obtained from the eigenvectors and the (square-roots of) eigenvalues of the dynamical matrix, respectively. The elements of the dynamical matrix are given by

$$D_{\alpha\beta}(\kappa, \kappa'; \mathbf{q}) = \frac{\sum_{l'} \Phi_{\alpha\beta}(l\kappa, l'\kappa') e^{-i\mathbf{q} \cdot \mathbf{x}_{l\kappa, l'\kappa'}}}{\sqrt{M_\kappa M_{\kappa'}}}, \quad (6)$$

where $\mathbf{x}_{l\kappa, l'\kappa'} = \mathbf{x}(l\kappa) - \mathbf{x}(l'\kappa')$, $\mathbf{x}(l\kappa) = \mathbf{x}(l) + \mathbf{x}(\kappa)$ is the position of atom $(l\kappa)$, $\mathbf{x}(l)$ is the position of unit cell l and $\mathbf{x}(\kappa)$ is the position of atom κ with respect to the origin in unit cell l , M_κ is the mass of atom κ and $\mathbf{q} = (q_x, q_y)$ is the phonon wave vector.

The definition in Eq. (6) differs from that of Ref. [19] in the phase factor: we use $\mathbf{x}(l\kappa) - \mathbf{x}(l'\kappa')$ instead of $\mathbf{x}(l) - \mathbf{x}(l')$. This difference in convention is physically inconsequential, but does affect some technical steps below. For example, the dynamical matrix in our case is not periodic under a translation by a reciprocal lattice vector \mathbf{G} :

$$D_{\alpha\beta}(\kappa, \kappa'; \mathbf{q} + \mathbf{G}) = e^{-i\mathbf{G} \cdot (\mathbf{x}(\kappa) - \mathbf{x}(\kappa'))} D_{\alpha\beta}(\kappa, \kappa'; \mathbf{q}). \quad (7)$$

From the elements $D_{\alpha\beta}(\kappa, \kappa'; \mathbf{q})$, the dynamical matrix

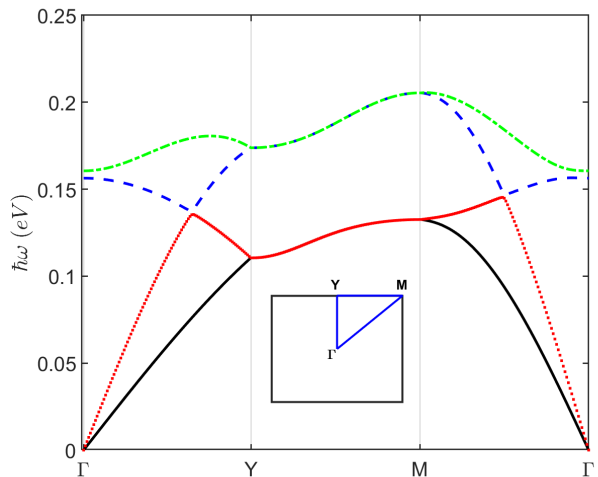


FIG. 2. Phonon dispersion along high symmetry directions indicated with blue triangle in the inset. The numerical values are $\gamma_0 = 200$ N/m, $\gamma_1 = 300$ N/m, $\gamma_2 = 280$ N/m, $M_1 = M_2 = 2 \times 10^{-26}$ kg, $\delta a = 0.2a$.

in the $(u_{1x}, u_{1y}, u_{2x}, u_{2y})$ basis is constructed as

$$D(\mathbf{q}) = \begin{pmatrix} D_{xx}(1,1) & D_{xy}(1,1) & D_{xx}(1,2) & D_{xy}(1,2) \\ & D_{yy}(1,1) & D_{yx}(1,2) & D_{yy}(1,2) \\ & & D_{xx}(2,2) & D_{xy}(2,2) \\ & & & D_{yy}(2,2) \end{pmatrix}, \quad (8)$$

where the lower-triangular terms in Eq. (8) are determined from the hermiticity condition $D(\mathbf{q}) = D^\dagger(\mathbf{q})$. The \mathbf{q} -dependence of the matrix elements in Eq. (8) has been left implicit for brevity of notation. The explicit expressions for $D_{\alpha\beta}(\kappa, \kappa'; \mathbf{q})$ were derived in Ref. [14] from Eq. (3) and are collected in App. A for reference.

Phonon bands calculated from Eq. (8) are shown in Fig. 2. One salient feature in the plot is the double degeneracy of the phonon dispersion along the YM line of the Brillouin zone edge (cf. Fig. 2), which, as we explain next, can be understood from the symmetry properties of the dynamical matrix.

Under a symmetry operation R , the dynamical matrix transforms as

$$\mathbf{\Gamma}(\mathbf{q}; R) D(\mathbf{q}) \mathbf{\Gamma}^{-1}(\mathbf{q}; R) = D(\mathbf{R} \cdot \mathbf{q}), \quad (9)$$

where \mathbf{R} is the (proper or improper) rotation matrix associated to the symmetry operation R and $\mathbf{\Gamma}$ is the representation matrix for the symmetry operator R . An explicit expression for $\mathbf{\Gamma}$ is given in Eq. (2.37) of Ref. [19], whose phase factor we must modify due to the different convention used in Eq. (6). Repeating the procedure of Ref. [19] with our convention, we find the phase factor of $\mathbf{\Gamma}$ to be $i(\mathbf{R} \cdot \mathbf{q}) \cdot (\mathbf{v} + \mathbf{x}(m))$, where \mathbf{v} is the fractional translation associated to the symmetry operation R ($\mathbf{v} = 0$ for a symmorphic operation) and $\mathbf{x}(m)$ is a translation vector of the crystal.

In case of the C_{2x} and $\sigma_v(xz)$ symmetries of BaMnSb₂, we have

$$\Gamma(\mathbf{q}; C_{2x}) = \begin{pmatrix} 1 & 0 & 0 & 0 \\ 0 & -1 & 0 & 0 \\ 0 & 0 & 1 & 0 \\ 0 & 0 & 0 & -1 \end{pmatrix} \quad (10)$$

in the $(u_{1x}, u_{1y}, u_{2x}, u_{2y})$ basis, as well as $\mathbf{R} \cdot \mathbf{q} = (q_x, -q_y)$. With this, it is easy to verify that the dynamical matrix elements shown in App. A satisfy Eq. (9). But this alone cannot explain the degeneracy of the phonon bands along YM. It turns out that the degeneracy is a consequence of an additional glide plane symmetry G_{2y} present in the lattice of Fig. 1 (despite it being absent in the space group of the 3D BaMnSb₂ crystal).

The operation G_{2y} consists of a translation along y by half of a unit cell, followed by a mirror reflection perpendicular to the x axis. The symmetry exchanges the two Sb atoms in the two dimensional unit cell. Then,

$$\Gamma(\mathbf{q}; G_{2y}) = e^{-iq_y b/2} \begin{pmatrix} 0 & 0 & -1 & 0 \\ 0 & 0 & 0 & 1 \\ -1 & 0 & 0 & 0 \\ 0 & 1 & 0 & 0 \end{pmatrix}, \quad (11)$$

where b is the lattice constant in the y direction. Also, $\mathbf{R} \cdot \mathbf{q} = (-q_x, q_y)$.

The last important symmetry to understand the degeneracy of the phonon modes along the YM line is \mathcal{T} -symmetry, which implies [19]

$$D(\mathbf{q}) = D(-\mathbf{q})^*. \quad (12)$$

Combining Eqs. (7), (9) and (10), the dynamical matrix along the YM line acquires the form

$$\begin{pmatrix} D_{xx}(1,1) & 0 & 0 & D_{xy}(1,2) \\ 0 & D_{yy}(1,1) & D_{yx}(1,2) & 0 \\ 0 & D_{yx}(1,2)^* & D_{xx}(2,2) & 0 \\ D_{xy}(1,2)^* & 0 & 0 & D_{yy}(2,2) \end{pmatrix}, \quad (13)$$

which can be immediately block diagonalized into two 2×2 blocks. We will now prove that the two blocks are identical because $D_{\alpha\alpha}(1,1; \mathbf{q}) = D_{\alpha\alpha}(2,2; \mathbf{q})$ and $D_{\alpha\beta}(1,2; \mathbf{q}) = D_{\beta\alpha}(1,2; \mathbf{q})$, thereby explaining the two double-degenerate phonon bands at the YM line in Fig. 2. To show this, we notice the following symmetry relations:

$$\begin{aligned} D_{\alpha\alpha}(\kappa, \bar{\kappa}; q_x, q_y) &\stackrel{G_{2y}}{=} D_{\alpha\alpha}(\bar{\kappa}, \bar{\kappa}; -q_x, q_y) \\ &\stackrel{\mathcal{T}}{=} D_{\alpha\alpha}(\bar{\kappa}, \bar{\kappa}; q_x, -q_y) \stackrel{C_{2x}}{=} D_{\alpha\alpha}(\bar{\kappa}, \bar{\kappa}; q_x, q_y)^* \\ &\stackrel{\text{hermiticity}}{=} D_{\alpha\alpha}(\bar{\kappa}, \bar{\kappa}; q_x, q_y), \end{aligned} \quad (14)$$

where κ and $\bar{\kappa}$ are different atoms (i.e. $\kappa = 1$ if $\bar{\kappa} = 2$, and $\kappa = 2$ if $\bar{\kappa} = 1$). The first equality of Eq. (14) has been derived from combining Eqs. (9) and (11). Thus, Eq. (14) proves that $D_{\alpha\alpha}(1,1; \mathbf{q}) = D_{\alpha\alpha}(2,2; \mathbf{q})$. Similarly, $D_{\alpha\beta}(1,2; \mathbf{q}) = D_{\beta\alpha}(1,2; \mathbf{q})$ follows directly from Eqs. (5) and (6).

We conclude this subsection by emphasizing that the space group of the actual BaMnSb₂ crystal is symmorphic [13]; i.e. it does not contain the G_{2y} operation. Thus, we will henceforth disregard G_{2y} , though it is possible to show that its presence would rule out the phonon helicity and the phonon Berry curvature.

B. Effective dynamical matrices

In this work, we are interested in long-wavelength (small- q) phonons. At $q = 0$, the dynamical matrix has two degenerate zero-frequency acoustic modes with eigenvectors

$$\begin{aligned} |A_{0,x}\rangle &= (1/\sqrt{2})(1, 0, 1, 0)^T \\ |A_{0,y}\rangle &= (1/\sqrt{2})(0, 1, 0, 1)^T \end{aligned} \quad (15)$$

and two nondegenerate optical modes with eigenvectors

$$\begin{aligned} |O_{0,x}\rangle &= (1/\sqrt{2})(1, 0, -1, 0)^T \text{ (} A_1 \text{ mode)} \\ |O_{0,y}\rangle &= (1/\sqrt{2})(0, 1, 0, -1)^T \text{ (} B_1 \text{ mode)}. \end{aligned} \quad (16)$$

At finite wave vectors, one must diagonalize $D(\mathbf{q})$ to obtain the phonon polarizations. Yet, an approximate analytical approach can be pursued for small q values (near the Γ point of Fig. 2), where the optical and acoustic phonon branches are well separated from one another in frequency. The approximation consists of decomposing the dynamical matrix in two decoupled 2×2 matrices, $D(\mathbf{q}) \simeq \mathcal{D}^a(\mathbf{q}) \oplus \mathcal{D}^o(\mathbf{q})$, where

$$\begin{aligned} \mathcal{D}^a(\mathbf{q}) &\equiv \begin{pmatrix} \langle A_{0,x} | D(\mathbf{q}) | A_{0,x} \rangle & \langle A_{0,x} | D(\mathbf{q}) | A_{0,y} \rangle \\ \langle A_{0,y} | D(\mathbf{q}) | A_{0,x} \rangle & \langle A_{0,y} | D(\mathbf{q}) | A_{0,y} \rangle \end{pmatrix} \\ \mathcal{D}^o(\mathbf{q}) &\equiv \begin{pmatrix} \langle O_{0,x} | D(\mathbf{q}) | O_{0,x} \rangle & \langle O_{0,x} | D(\mathbf{q}) | O_{0,y} \rangle \\ \langle O_{0,y} | D(\mathbf{q}) | O_{0,x} \rangle & \langle O_{0,y} | D(\mathbf{q}) | O_{0,y} \rangle \end{pmatrix} \end{aligned} \quad (17)$$

are the effective acoustic and optical dynamical matrices. They can be written as

$$\mathcal{D}^{a/o} = d_0^{a/o} \sigma_0 + \sum_{i=x,y,z} d_i^{a/o} \sigma_i, \quad (18)$$

where σ_i is the effective pseudospin in the $\{x, y\}$ basis. Starting from the expressions for $D_{\alpha\beta}(\kappa, \bar{\kappa}; \mathbf{q})$ in App. A and doing a small q approximation, we obtain

$$\begin{aligned} d_0^{a(o)} &\simeq \frac{1}{M} \left[\gamma_+ \left(1 \mp \left(1 - \frac{q^2}{8} \right) \right) + \gamma_0 \frac{q^2}{2} \right] \\ d_z^{a(o)} &\simeq \frac{1}{M} \left[\gamma_- \delta a \left(1 \mp \left(1 - \frac{q^2}{8} \right) \right) + \gamma_0 \frac{q_x^2 - q_y^2}{2} \right] \\ d_x^{a(o)} &\simeq \pm \frac{1}{M} \gamma_+ \frac{q_x q_y}{4} \\ d_y^{a(o)} &= 0, \end{aligned} \quad (19)$$

where M is the mass of an Sb atom, $\gamma_{\pm} \equiv \gamma_2 \pm \gamma_1$ and we have assumed that the zig-zag distortion (δa) is small.

The upper (lower) signs in Eq. (19) correspond to acoustic (optical) modes.

Symmetry wise, projecting Eq. (9) onto the optical ($\{O_{0,x}\}, \{O_{0,y}\}$) or acoustic ($\{A_{0,x}\}, \{A_{0,y}\}$) subspaces, we get the constraint

$$\sigma_z \mathcal{D}^{o/a}(q_x, q_y) \sigma_z = \mathcal{D}^{o/a}(q_x, -q_y) \quad (20)$$

from the C_{2x} or $\sigma_v(xz)$ symmetries, which is satisfied by Eq. (19).

C. Berry curvature

In this section, we calculate the Berry curvature for long-wavelength acoustic and optical phonons in BaMnSb₂, in the absence of the coupling to Dirac fermions. The first step is to obtain the effective phonon Hamiltonian. As shown in Ref. [10], an effective Hamiltonian for phonons can be written as

$$\mathcal{H}_{\text{ph}}(\mathbf{q}) = \mathcal{D}^{1/2}(\mathbf{q}) + i\mathcal{G}(\mathbf{q}), \quad (21)$$

where $\mathcal{G}(\mathbf{q})$ is the molecular Berry curvature [12] projected onto the acoustic or optical phonon subspaces. As shown explicitly in App. B, $\mathcal{G}(\mathbf{q})$ vanishes due to time-reversal symmetry. There exist alternative expressions for the effective phonon Hamiltonian in the literature [1, 2, 20], depending on whether the Hamiltonian is written in terms of the canonical or mechanical momenta. All these expressions are unitarily equivalent when $\mathcal{G} = 0$, which is the situation that interests us here.

Thus, the effective 2×2 Hamiltonians for acoustic and optical phonons are simply the square roots of \mathcal{D}^a and \mathcal{D}^o , respectively. Omitting for brevity the superscripts a and o , as well as the wave vector label \mathbf{q} , it is easy to show that

$$\mathcal{H}_{\text{ph}} = \mathcal{D}^{1/2} = V \mathbb{D}^{1/2} V^\dagger, \quad (22)$$

where V is a unitary matrix that diagonalizes \mathcal{D} ,

$$\mathbb{D} = V^\dagger \mathcal{D} V = \begin{pmatrix} d_0 + d & 0 \\ 0 & d_0 - d \end{pmatrix} \equiv \begin{pmatrix} \omega_1^2 & 0 \\ 0 & \omega_2^2 \end{pmatrix} \quad (23)$$

is the diagonalized effective dynamical matrix for the acoustic or optical modes, and d is the modulus of $\mathbf{d} = (d_x, d_y, d_z)$ listed in Eq. (19). Using $\mathbb{D}^{1/2} = \text{diag}(\omega_1, \omega_2)$ and [21]

$$V = \begin{pmatrix} \cos \frac{\theta}{2} & \sin \frac{\theta}{2} e^{-i\phi} \\ \sin \frac{\theta}{2} e^{i\phi} & -\cos \frac{\theta}{2} \end{pmatrix} \quad (24)$$

with $\cos \theta = d_z/d$ and $\tan \phi = d_y/d_x$, Eq. (22) becomes

$$\mathcal{H}_{\text{ph}} = h_0 \sigma_0 + \sum_{i=x,y,z} h_i \sigma_i, \quad (25)$$

where

$$\begin{aligned} h_0 &= \frac{\omega_1 + \omega_2}{2} \\ h_i &= \frac{\omega_1 - \omega_2}{2d} d_i. \end{aligned} \quad (26)$$

Here, σ_i is once again the pseudospin the $\{x, y\}$ basis. A few remarks are in order: (i) For the effective Hamiltonian to be defined, we should have $d_0 > d$, i.e. the eigenvalues of the dynamical matrix must be non-negative; (ii) the eigenvalues of the effective Hamiltonian are the phonon frequencies ω_1 and ω_2 ; (iii) the eigenvectors of \mathcal{H}_{ph} coincide with those of \mathcal{D} .

From Eq. (25), the Berry curvature can be obtained using [22]

$$\Omega_{\pm}(\mathbf{q}) = \pm \hat{\mathbf{z}} \frac{1}{2h^3} \mathbf{h} \cdot (\partial_{q_x} \mathbf{h} \times \partial_{q_y} \mathbf{h}), \quad (27)$$

where $\mathbf{h} = (h_x, h_y, h_z)$, \pm corresponds to the two acoustic or optical in-plane phonon modes, and h is the modulus of \mathbf{h} .

Combining Eqs. (26) and (27) immediately gives $\Omega_{\pm}(\mathbf{q}) = 0$. The mathematical reason for it is that $h_y = 0$ in Eq. (26), because $d_y = 0$ in Eq. (19). Indeed, h_x, h_y and h_z must all be nonzero for a Berry curvature to emerge. Thus, *bare* phonons in BaMnSb₂ do not have any Berry curvature.

From more physical viewpoint, the underlying reason for the vanishing of the Berry curvature is that our force constant model obeys Eq. (5). This condition leads to $h_y = 0$. To see that, it suffices to show that the off-diagonal element of $\mathcal{D}^{o,a}$, denoted here as $\mathcal{D}_{xy}^{o,a}$, is purely real. From Eqs. (8) and (17), we have

$$\begin{aligned} \mathcal{D}_{xy}^{o,a}(\mathbf{q}) &= \frac{1}{2} [\mp D_{xy}(1, 2) \mp D_{yx}^*(1, 2) \\ &\quad + D_{xy}(1, 1) + D_{xy}(2, 2)]. \end{aligned} \quad (28)$$

If Eq. (5) is obeyed, then it follows from Eq. (6) that $D_{xy}(1, 2) = D_{yx}(1, 2)$. Consequently, the first line of Eq. (28) is purely real. The second line is likewise purely real, because Eq. (5) implies $D_{xy}(\kappa, \kappa) = D_{yx}(\kappa, \kappa)$, whereas hermiticity of the dynamical matrix in Eq. (8) imposes $D_{yx}(\kappa, \kappa) = D_{xy}(\kappa, \kappa)^*$. Thus, $D_{xy}(\kappa, \kappa)$ must be a real number.

In sum, force constants satisfying Eq. (5) preclude a phonon Berry curvature. As we show next, the coupling between phonons and Dirac fermions changes this state of affairs, by effectively providing force constants $\Phi_{\alpha\beta}(l\kappa, l'\kappa')$ that are not symmetric under exchange of α and β .

IV. ELECTRON-PHONON INTERACTION

Because the low-energy electronic states originate mainly from Sb layers, they couple significantly to the vibrations of Sb atoms. The unscreened electron-phonon interaction Hamiltonian reads [23, 24]

$$\mathcal{H}_{\text{e-ph}} = \sum_{\mathbf{q}, \mathbf{k}} \sum_{\lambda, s, \alpha, \beta} g_{\alpha, \beta}^{\lambda, s}(\mathbf{q}) u_{\mathbf{q}, \lambda} c_{s, \alpha, \mathbf{k}}^\dagger c_{s, \beta, \mathbf{k} - \mathbf{q}}, \quad (29)$$

where $u_{\mathbf{q}, \lambda} = (b_{\mathbf{q}, \lambda} + b_{-\mathbf{q}, \lambda}^\dagger) / \sqrt{4M\omega_{\mathbf{q}, \lambda}}$ is the phonon displacement operator, $2M$ is the mass of two Sb atoms in

the unit cell, $b_{\mathbf{q},\lambda}$ is an operator that annihilates a phonon mode λ with momentum \mathbf{q} , α, β represent electronic p -orbitals and $g_{\alpha,\beta}^{\lambda,s}$ is the electron-phonon matrix element; only valley-preserving (i.e. long-wavelength) phonons are considered, such that we may write $\mathcal{H}_{e\text{-ph}} = \sum_s \mathcal{H}_{e\text{-ph}}^s$. The 2×2 electron-phonon coupling matrix at valley s satisfies the hermiticity condition

$$g^{\lambda,s}(\mathbf{q})^\dagger = g^{\lambda,s}(-\mathbf{q}) \quad (30)$$

and the time-reversal symmetry condition

$$g^{\lambda,s}(\mathbf{q}) = [g^{\lambda,-s}(-\mathbf{q})]^*. \quad (31)$$

The dependence of $g_{\alpha,\beta}^{\lambda,s}$ on \mathbf{k} (the electronic wave vector measured from a given valley s) is neglected, but its valley-dependence is considered through the label s . The form of the allowed terms in $g_{\alpha,\beta}^{\lambda,s}$ can be determined from symmetry analysis [14].

In this study, we focus only on the interaction between the low-energy Dirac fermions and the phonons. Moreover, we concentrate on the deformation potential coupling for optical and acoustic phonons, thereby neglecting the Frölich and the piezoelectric interactions [25, 26].

A. Optical deformation potential

The optical deformation potential matrix $g^{\lambda,s}$ can be approximated to be independent of \mathbf{q} for long-wavelength optical phonons. This approximation is enabled by the fact that the two $q = 0$ optical modes of interest, $|O_{0,x}\rangle$ (A_1) and $|O_{0,y}\rangle$ (B_1) in Eq. (16), are not degenerate. The invariance of $\mathcal{H}_{e\text{-ph}}^s$ under the combined symmetry $C_{2x}\mathcal{T}$ then implies [14]

$$\tau_z (g^{\lambda,s})^* \tau_z = x_\lambda g^{\lambda,s}, \quad (32)$$

where Eq. (16) has been used through

$$(C_{2x}\mathcal{T})u_{0,\lambda}(C_{2x}\mathcal{T})^{-1} = x_\lambda u_{0,\lambda} \quad (33)$$

with $x_{A_1} = +1$ and $x_{B_1} = -1$. For a given valley $s \in \{+, -\}$, Eqs. (32), (31) and (30) lead to

$$\begin{aligned} g^{A_1,s} &= g_0^o \tau_0 + s g_y^o \tau_y + g_z^o \tau_z \\ g^{B_1,s} &= g_x^o \tau_x, \end{aligned} \quad (34)$$

where $g_{0,1,2,3}^o$ are real \mathbf{q} -independent numbers.

B. Acoustic deformation potential

Acoustic phonons become degenerate at $q \rightarrow 0$. For that reason, as soon as q becomes infinitesimally nonzero, $|A_{0,x}\rangle$ and $|A_{0,y}\rangle$ are no longer the eigenmodes of the dynamical matrix for a generic $\hat{\mathbf{q}}$ (not even approximately so); the eigenmodes must instead be obtained from diagonalizing \mathcal{D}^a . For simplicity, we will approximate the two

in-plane acoustic modes in the $q \rightarrow 0$ limit as longitudinal (LA) and transverse (TA), with polarization vectors

$$\begin{aligned} \mathbf{p}_{\hat{\mathbf{q}},LA} &= \hat{\mathbf{q}} \\ \mathbf{p}_{\hat{\mathbf{q}},TA} &= \hat{\mathbf{q}} \times \hat{\mathbf{z}}. \end{aligned} \quad (35)$$

The exact polarizations, obtained by diagonalizing \mathcal{D}^a in the $q \rightarrow 0$ regime, tend to Eq. (35) under the assumption of isotropy (neglect of δa and assumption of $\gamma_0 = \gamma_+/4$). For qualitative purposes, this approximation is satisfactory when the zig-zag distortion is small. For analytical convenience, we will continue to use Eq. (35).

From the acoustic sum rule, we know that $g^{\lambda,s}(\mathbf{q})$ must vanish when $q \rightarrow 0$. Taylor-expanding the microscopic expression for the electron-phonon matrix elements (found e.g. in the Supplemental Material of [14]) in powers of q , the leading order deformation potential term is of the form

$$g^{\lambda,s}(\mathbf{q}) = \sum_{\nu,\nu'} \Xi_{\nu,\nu'}^{\lambda,s} q_\nu \mathbf{p}_{\hat{\mathbf{q}},\nu'}, \quad (36)$$

where $\nu, \nu' \in \{x, y\}$ and $\Xi_{\nu,\nu'}^{\lambda,s}$ is a \mathbf{q} -independent 2×2 matrix.

If we assume isotropy, the only two vectors governing $g^{\lambda,s}(\mathbf{q})$ are \mathbf{q} and $\mathbf{p}_{\hat{\mathbf{q}},\lambda}$. Since the electron-phonon matrix elements are scalars, they must involve either $\mathbf{q} \cdot \mathbf{p}_{\hat{\mathbf{q}},\lambda}$ or $(\mathbf{q} \times \hat{\mathbf{z}}) \cdot \mathbf{p}_{\hat{\mathbf{q}},\lambda}$ (the only two scalars that can be formed from the aforementioned two vectors, $\hat{\mathbf{z}}$ being the unit vector normal to the Sb planes). Then, Eq. (36) can be simplified to

$$g^{\lambda,s}(\mathbf{q}) = \Xi^{LA,s} \mathbf{q} \cdot \mathbf{p}_{\hat{\mathbf{q}},\lambda} + \Xi^{TA,s} (\mathbf{q} \times \hat{\mathbf{z}}) \cdot \mathbf{p}_{\hat{\mathbf{q}},\lambda}, \quad (37)$$

where the first (second) term in the right hand side only appears for the longitudinal (transverse) mode. As a result,

$$g^{\lambda,s}(\mathbf{q}) = \Xi^{\lambda,s} q, \quad (38)$$

where $\Xi^{\lambda,s}$ is a q -independent 2×2 matrix. For similar approximations in related systems, see e.g. Refs. [27, 28].

In order to identify the nonzero elements of the deformation potential matrix $\Xi^{\lambda,s}$, we use symmetry arguments. First, we recognize that

$$(C_{2x}\mathcal{T})\mathbf{p}_{\hat{\mathbf{q}},\lambda}(C_{2x}\mathcal{T})^{-1} = x_\lambda \mathbf{p}_{(C_{2x}\mathcal{T})\hat{\mathbf{q}},\lambda}, \quad (39)$$

with $x_{LA} = -1$ and $x_{TA} = +1$. Using the invariance of $\mathcal{H}_{e\text{-ph}}^s$ under $C_{2x}\mathcal{T}$ and keeping in mind that $u_{\mathbf{q},\lambda}$ transforms in the same way as $\mathbf{p}_{\hat{\mathbf{q}},\lambda}$ under symmetry operations, we have

$$\tau_z (g^{\lambda,s}(q_x, q_y))^* \tau_z = x_\lambda g^{\lambda,s}(-q_x, q_y). \quad (40)$$

Combining this with Eqs. (30) and (31), we get

$$\begin{aligned} \Xi^{LA,s} &= g_x^a \tau_x \\ \Xi^{TA,s} &= g_0^a \tau_0 + s g_y^a \tau_y + g_z^a \tau_z, \end{aligned} \quad (41)$$

where $g_{0,1,2,3}^a$ are real \mathbf{q} -independent numbers.

V. DRESSED IN-PLANE PHONONS

A. Dynamical matrix

The electron-phonon interaction of Sec. IV modifies the phonon frequencies and eigenvectors calculated in Sec. III. In this section, we will find out how the effective 2×2 dynamical matrices \mathcal{D}^a and \mathcal{D}^o for the acoustic and optical modes are modified in the presence of electron-phonon interactions. We will neglect the hybridization between optical and acoustic modes caused by electrons, instead concentrating on the changes occurring within the optical and acoustic mode subspaces. One convenient way to identify these changes is from the effective action for optical or acoustic phonons, obtained by integrating out the Dirac fermions. We have detailed this procedure in Ref. [17]. Here, we simply quote the outcome,

$$S_{\text{eff}} = \frac{Mk_B T}{\mathcal{S}} \sum_{\mathbf{q}, q_m} (u_{\mathbf{q},1}^*(q_m), u_{\mathbf{q},2}^*(q_m)) \times \begin{pmatrix} q_m^2 + \omega_1^2 + \Sigma_{11} & \Sigma_{12} \\ \Sigma_{21} & q_m^2 + \omega_2^2 + \Sigma_{22} \end{pmatrix} \begin{pmatrix} u_{\mathbf{q},1}(q_m) \\ u_{\mathbf{q},2}(q_m) \end{pmatrix}, \quad (42)$$

where T is the temperature, k_B is the Boltzmann constant, q_m a bosonic Matsubara frequency, \mathcal{S} the sample area and $\Sigma_{\lambda\lambda'}$ is an element of the phonon self-energy (dependent on \mathbf{q} and q_m) caused by its coupling to electrons. The subscripts 1 and 2 label the two in-plane, bare acoustic or optical phonons: in the case of optical phonons, 1 (2) corresponds to the A_1 (B_1) mode; in the case of acoustic phonons, 1 (2) corresponds to the longitudinal L (transverse T) mode.

We will be interested in the low-temperature regime, and in phonon frequencies lower than the electronic bandgap. In that regime, $\Sigma_{\lambda\lambda}$ is purely real and can be simply absorbed into ω_λ . Concerning the off-diagonal self-energies, their low-frequency and long-wavelength expansion reads

$$\Sigma_{AB} = -\Sigma_{BA} \simeq -\frac{g_0^o g_x^o}{M} \frac{iq_y}{2\pi v_0} \text{sgn}(m_0) \quad (43)$$

for the case of optical phonons. For acoustic phonons, the corresponding expressions are

$$\Sigma_{TL} = -\Sigma_{LT} \simeq -\frac{g_0^a g_x^a}{M} \frac{iq^2 q_y}{2\pi v_0} \text{sgn}(m_0). \quad (44)$$

In Eqs. (43) and (44), the valley electronic Chern number $\text{sgn}(m_0)$ enters directly. The off-diagonal self-energies are static to leading order (i.e. they are finite at $q_m \rightarrow 0$). In addition, the fact that these terms are imaginary renders the dressed phonons helical [14], with an angular momentum along the z direction that inverts sign under $q_y \rightarrow -q_y$. Finally, the bare values of $g_0^o g_x^o$ and $g_0^a g_x^a$ must be divided by the dielectric constant ϵ in order to account for electron-electron interactions in the random phase approximation.

The equation of motion for the phonon dynamics can be obtained by minimizing the effective action:

$$\frac{\delta S_{\text{eff}}}{\delta u_{\mathbf{q},\lambda}(q_m)} = 0 \quad (45)$$

for $\lambda = 1, 2$. This yields

$$(iq_m)^2 \begin{pmatrix} u_{\mathbf{q},1}(q_m) \\ u_{\mathbf{q},2}(q_m) \end{pmatrix} = \tilde{\mathbb{D}}(\mathbf{q}) \begin{pmatrix} u_{\mathbf{q},1}(q_m) \\ u_{\mathbf{q},2}(q_m) \end{pmatrix}, \quad (46)$$

where

$$\tilde{\mathbb{D}}(\mathbf{q}) = \begin{pmatrix} \omega_1^2 + \Sigma_{11} & \Sigma_{12} \\ -\Sigma_{12} & \omega_2^2 + \Sigma_{22} \end{pmatrix} \quad (47)$$

is the renormalized effective dynamical matrix for in-plane optical ($1 = A, 2 = B$) or in-plane acoustic ($1 = L, 2 = T$) modes.

It is important to note that this dynamical matrix is written in the eigenbasis $\{1, 2\}$ of the bare phonons, whereas the one obtained in Eq. (18) is in the $\{x, y\}$ basis. We therefore carry out a unitary transformation $\tilde{\mathcal{D}} = W \tilde{\mathbb{D}} W^\dagger$, where W is given by Eq. (24) for the case of optical phonons and

$$W = \begin{pmatrix} \hat{\mathbf{q}} \cdot \hat{\mathbf{x}} & -\hat{\mathbf{q}} \cdot \hat{\mathbf{y}} \\ \hat{\mathbf{q}} \cdot \hat{\mathbf{y}} & \hat{\mathbf{q}} \cdot \hat{\mathbf{x}} \end{pmatrix} \quad (48)$$

for the case of acoustic phonons. After performing the transformation, we have the renormalized effective dynamical matrices for the acoustic and optical modes in the $\{x, y\}$ basis:

$$\tilde{\mathcal{D}}^{a/o} = \tilde{d}_0^{a/o} \sigma_0 + \sum_{i=x,y,z} \tilde{d}_i^{a/o} \sigma_i, \quad (49)$$

where

$$\begin{aligned} \tilde{d}_0^{o(a)} &= d_0^{o(a)} + \frac{\Sigma_{11} + \Sigma_{22}}{2} \\ \tilde{d}_z^{o(a)} &= d_z^{o(a)} \left(1 + \frac{\Sigma_{11} - \Sigma_{22}}{2d^{o(a)}} \right) \\ \tilde{d}_x^{o(a)} &= d_x^{o(a)} \left(1 + \frac{\Sigma_{11} - \Sigma_{22}}{2d^{o(a)}} \right) \\ \tilde{d}_y^{o(a)} &= \pm \text{Im} \Sigma_{12}. \end{aligned} \quad (50)$$

The diagonal phonon self-energy terms Σ_{11} and Σ_{22} simply renormalize the spring constants appearing in the dynamical matrix of the bare phonons. In contrast, the imaginary off-diagonal self-energy Σ_{12} leads to new physical effects that cannot be accounted for using the bare spring constants of Sec. III.

In density functional theory [7, 29], the imaginary off-diagonal phonon self-energy and the corresponding phonon helicity should be obtainable within the adiabatic (Born-Oppenheimer) approximation with dressed force constants, because said self-energy has been computed in the static ($q_m \rightarrow 0$) limit. Yet, the various empirical force-constant models we have used to obtain the

dynamical matrix of Sec. III fail to predict phonon helicity. Indeed, as we proved in Sec. III, $\hat{d}_y = 0$ if the force constant matrix obeys Eq. (5). It is therefore clear that the coupling of Dirac fermions to lattice vibrations violates Eq. (5) by contributing terms to the renormalized force constants that are *asymmetric* under the exchange of α and β . Such terms, proportional to the electronic valley Chern number, generate phonon helicity.

Another key aspect of the off-diagonal phonon self-energy is that it generates a phonon Berry curvature. In Sec. III C, we observed that the Berry curvature of bare phonons was zero due to $d_y = 0$ in Eq. (18). Now that $\hat{d}_y \neq 0$, we expect the dressed phonons to have a nonzero Berry curvature.

B. Berry curvature

Let us again calculate the Berry curvature for phonons, as in Sec. III C, but this time using the effective Hamiltonian of dressed phonons. For the optical modes, we get

$$\Omega_{\pm}(\mathbf{q}) \simeq \pm \hat{\mathbf{z}} \frac{M\gamma_+ \text{sign}(\gamma_- \delta a)}{32\gamma_-^2 \delta a^2} \text{Im}\Sigma_{AB}, \quad (51)$$

where we have expanded in powers of q first and afterwards assumed that $\gamma_- \delta a \ll \gamma_+$ (weak zig-zag distortion). For the acoustic modes, we get

$$\Omega(\mathbf{q}) \simeq \pm \hat{\mathbf{z}} \frac{2M}{\gamma_0 q^4} \text{Im}\Sigma_{LT}, \quad (52)$$

where we have adopted the isotropic approximation from the onset (neglecting δa and assuming $\gamma_+ = 4\gamma_0$). The main conclusion from these expressions is that Berry curvature of the dressed optical and acoustic phonons is proportional to the phonon helicity and thus to the electronic valley Chern number. In some sense, phonons have *inherited* the Berry curvature from electrons through the electron-phonon interactions. This is the main result from the present work.

The phonon Berry curvature obeys $\Omega(\mathbf{q}) = -\Omega(-\mathbf{q})$, $\Omega(q_x, q_y) = -\Omega(q_x, -q_y)$ and $\Omega(q_x, q_y) = \Omega(-q_x, q_y)$, which are consistent with the \mathcal{T} , C_{2x} and $C_{2x}\mathcal{T}$ symmetries of the crystal, respectively. One way to detect this Berry curvature is to break time-reversal symmetry with a magnetic field and to measure a thermal Hall effect of phonons.

VI. EFFECT OF A TIME-REVERSAL BREAKING PERTURBATION

A. Berry curvature of dressed in-plane phonons

In this section, we revisit the Berry curvature for optical and acoustic modes in the presence of a time-reversal

breaking perturbation. For simplicity, we will limit ourselves to the effect of a ferromagnetic exchange field B along the z direction, whose effect on the electronic structure can be captured through a valley Zeeman splitting. An explicit calculation in App. B shows that, in our model, the molecular Berry curvature \mathcal{G} remains null in the presence of a valley Zeeman splitting, insofar as the latter is not strong enough to induce a band inversion in one of the valleys. Therefore, we can still use the formulae of Sec. III C to compute the phonon Berry curvature. The same qualitative effect would apply if we replaced the exchange field by a magnetic field and neglected the orbital effect (Landau-level splitting) due to the field.

In order to find out how B influences the phonon Berry curvature, we need to determine how it enters the phonon effective Hamiltonian. We will do so at the phenomenological level using symmetry arguments.

Finite $B \neq 0$ breaks the C_{2x} , $\sigma_v(xy)$, and \mathcal{T} symmetries of BaMnSb₂. Accordingly, the counterparts of Eqs. (12) and (20) read

$$\begin{aligned} \mathcal{D}^*(\mathbf{q}, B) &= \mathcal{D}(-\mathbf{q}, -B) \\ \sigma_z \mathcal{D}(q_x, q_y, B) \sigma_z &= \mathcal{D}(q_x, -q_y, -B). \end{aligned} \quad (53)$$

The hermiticity condition $\mathcal{D}^\dagger(\mathbf{q}, B) = \mathcal{D}(\mathbf{q}, B)$ holds unchanged.

For weak \mathcal{T} -breaking perturbations, we expand the dynamical matrix to the leading order in B ,

$$\mathcal{D}(\mathbf{q}, B) \simeq \mathcal{D}^0(\mathbf{q}) + \delta\mathcal{D}(\mathbf{q})B, \quad (54)$$

where $\mathcal{D}^0(\mathbf{q})$ is the dynamical matrix at $B = 0$ as in Eqs. (50). Owing to the hermiticity condition, we can express

$$\delta\mathcal{D}(\mathbf{q}) = \sum_i a_i(\mathbf{q}) \sigma_i \quad (55)$$

in terms of Pauli matrices ($i = 0, x, y, z$), $a_i(\mathbf{q})$ being a real and B -independent function of \mathbf{q} . To obey Eq. (53), a_0 and a_z must be odd functions of q_y and even functions of q_x ; a_x must be an odd function of q_x and an even function of q_y ; a_y must be an even function of both q_x and q_y . Keeping these constraints, we expand the coefficients a_i to leading order in q_x and q_y in the long-wavelength approximation. We also impose the requirement that $a_i \rightarrow 0$ when $q \rightarrow 0$ for acoustic phonons.

We recompute the Berry curvatures for optical and acoustic phonons from Eq. (54), Taylor-expanding first on q , then on B and finally on δa . The leading order correction to Eq. (51) for optical phonons reads

$$\delta\Omega \simeq \pm \hat{\mathbf{z}} \frac{3M^3 a \gamma_+ \text{sign}(\gamma_- \delta a)}{128\gamma_-^4 \delta a^4} (\text{Im}\Sigma_{AB})^2 B + \dots, \quad (56)$$

where a is the leading (q -independent) part of a_y . In Eq. (56), we have omitted terms that are smaller by a factor of $\gamma_- \delta a$. Those omitted terms are not proportional to Σ_{AB} . As a result, it is not required that the optical phonons be helical for them to acquire a Berry curvature when $B \neq 0$.

For the acoustic phonons, the leading order correction to Eq. (52) reads

$$\delta\Omega = \pm\hat{\mathbf{z}} \frac{24\hat{b}M^3}{\gamma_0^3 q^6} (\text{Im}\Sigma_{LT})^2 B + \dots, \quad (57)$$

where \hat{b} is the q -independent coefficient in a_y (assumed to be of the form $a_y \simeq \hat{b}(q_x^2 + q_y^2)$). The omitted terms in Eq. (57) originate from a_x and a_z . All the terms linear in B vanish in the absence of phonon helicity (i.e. when $\Sigma_{LT} = 0$).

Combining Eqs. (57) and (56) with Eqs. (52) and (51), we see that the total Berry curvatures of optical and acoustic phonons verify $\mathbf{\Omega}(q_x, q_y, B) = -\mathbf{\Omega}(q_x, -q_y, -B)$ and $\mathbf{\Omega}(q_x, q_y, B) = -\mathbf{\Omega}(-q_x, -q_y, -B)$. These relations are consistent with the way $\mathbf{\Omega}(\mathbf{q}, B)$ transforms under C_{2x} and \mathcal{T} .

B. Thermal Hall effect

Since the Berry curvature is no longer an odd function of q_y when $B \neq 0$, it makes a nonvanishing contribution to the thermal Hall conductivity κ_{xy} through a term [2, 30–32]

$$\kappa_{xy}^{\text{Berry}} = -\frac{k_B^2 T}{\hbar S} \sum_{\mathbf{q}, \lambda} f[\rho(\omega_{\mathbf{q}, \lambda})] \Omega_\lambda(\mathbf{q}), \quad (58)$$

where $\rho(\omega) = (e^{\hbar\omega/k_B T} - 1)^{-1}$ is the Bose-Einstein distribution function, $\omega_{\mathbf{q}, \lambda}$ is the phonon frequency, and $f(x) = (1+x)(\ln[(1+x)/x])^2 - (\ln x)^2 - 2\text{Li}_2(-x)$ with $\text{Li}_2(x)$ as the polylogarithm function of second order.

At low temperature, the phononic thermal Hall response is dominated by long-wavelength acoustic phonons. The frequencies of the latter are obtained from the effective dynamical matrix \mathcal{D}^a :

$$\omega_{\lambda, \mathbf{q}} \simeq c_\lambda q, \quad (59)$$

where $c_T = (\gamma_0/2M)^{1/2}$ and $c_L = \sqrt{3}c_T$ are the sound velocities for the longitudinal and transverse modes. In Eq. (59), we have neglected $O(B^2)$ corrections.

Replacing Eqs. (59) and (57) in Eq. (58), using $S^{-1} \sum_{\mathbf{q}} \propto \int dq q \int_0^{2\pi} d\chi$ with χ the polar angle of \mathbf{q} , making a change of variables $c_\lambda q/(k_B T) \rightarrow y$, and recognizing that $\delta\Omega_z$ in Eq. (57) is independent of q (and also T , if the temperature is well below the energy gap of the insulator), it is easy to see that $\kappa_{xy}^{\text{Berry}}$ scales as T^3 at low temperature. In addition, $\kappa_{xy}^{\text{Berry}}$ is proportional to the square of the *electronic* valley Chern number.

VII. SUMMARY AND CONCLUSIONS

To summarize, taking BaMnSb₂ as a prototypical \mathcal{T} -symmetric Dirac insulator, we have shown that phonons

acquire a Berry curvature by virtue of their coupling to Dirac fermions. The phonon Berry curvature being proportional to the electronic valley Chern number, we have characterized it as being “inherited”. This inherited Berry curvature is fundamentally different from the so-called molecular Berry curvature, which is an electronic Berry curvature resulting from ionic displacements in materials lacking \mathcal{T} -symmetry. While our calculation has concentrated on a low-energy effective model for BaMnSb₂, a similar effect could be realized in other \mathcal{T} -symmetric two-dimensional and three-dimensional materials with nontrivial electronic topology.

A legitimate critique for the present work concerns our definition of the “bare” phonons in Sec. III. To describe the lattice vibrations in the absence of the coupling to Dirac fermions, we have adopted a phenomenological force constant matrix that is symmetric under the interchange of the cartesian indices (Eq. (5)). We have shown that this symmetry results in phonons that do not have a Berry curvature. While the type of phenomenological model we have employed is commonplace, we have no proof that it is satisfactory to describe the phonons of BaMnSb₂ in the absence of Dirac fermions. In other words, while we can attest that Dirac fermions in BaMnSb₂ generate a phonon helicity and a phonon Berry curvature, we cannot assert that the latter originate *exclusively* from the Dirac fermions. This issue can be settled by first-principles calculations of the phonon dispersion and polarizations.

Another avenue for future work consists of exploring the possibility in which topologically trivial bare electrons would acquire a Berry curvature through their coupling to topologically nontrivial phonons. This effect would be converse to the one discussed in the present paper. While phonon-induced electronic topological transitions were predicted earlier [33], we are not aware of instances in which the electronic Berry curvature is known to emerge from the electron-phonon interaction.

ACKNOWLEDGMENTS

The authors acknowledge funding from the Canada First Research Excellence Fund and the Natural Sciences and Engineering Research Council of Canada (Grants No. RGPIN-2018-05385 and RGPIN-2024-05210). S. G. thanks the Department of Science and Technology (DST) for their financial support through Project No. SR/FST/PSI/2017/5(C).

Appendix A: Dynamical matrix for bare in-plane phonons

For reference, the explicit expressions for the non-null elements of the dynamical matrix in Eq. (8) are as follows:

$$\begin{aligned}
D_{xx}(1,1) &= \frac{2}{M} \left[\gamma_2 \left(\frac{\delta a + 1}{A} \right)^2 + \gamma_1 \left(\frac{\delta a - 1}{B} \right)^2 + \gamma_0(1 - \cos q_x) \right] \\
D_{yy}(1,1) &= \frac{2}{M} \left[\gamma_2 \left(\frac{1}{A} \right)^2 + \gamma_1 \left(\frac{1}{B} \right)^2 + \gamma_0(1 - \cos q_y) \right] \\
D_{xx}(1,2) &= \frac{2}{M} \cos \frac{q_y}{2} \left[-\gamma_2 \left(\frac{\delta a + 1}{A} \right)^2 e^{i \frac{q_x}{2} (\delta a + 1)} - \gamma_1 \left(\frac{\delta a - 1}{B} \right)^2 e^{i \frac{q_x}{2} (\delta a - 1)} \right] \\
D_{yy}(1,2) &= \frac{2}{M} \cos \frac{q_y}{2} \left[-\gamma_2 \left(\frac{1}{A} \right)^2 e^{i \frac{q_x}{2} (\delta a + 1)} - \gamma_1 \left(\frac{1}{B} \right)^2 e^{i \frac{q_x}{2} (\delta a - 1)} \right] \\
D_{xy}(1,2) &= i \frac{2}{M} \sin \frac{q_y}{2} \left[-\gamma_2 \left(\frac{\delta a + 1}{A^2} \right) e^{i \frac{q_x}{2} (\delta a + 1)} - \gamma_1 \left(\frac{\delta a - 1}{B^2} \right) e^{i \frac{q_x}{2} (\delta a - 1)} \right] \\
D_{xx}(2,2) &= D_{xx}(1,1) \\
D_{yy}(2,2) &= D_{yy}(1,1) \\
D_{yx}(1,2) &= D_{xy}(1,2),
\end{aligned} \tag{A1}$$

with $A = \sqrt{1 + (1 + \delta a)^2}$ and $B = \sqrt{1 + (1 - \delta a)^2}$. These results were first obtained in Ref. [14] using a force-constant model with only bond-stretching contributions to the lattice potential energy. Only force-constants between first and second-nearest neighbors were kept, and the unit cell was approximated as a square (of unit length in the equations above).

In the present work, we have considered two more general models: (1) a model that extends the one of Ref. [14] by keeping up to third-neighbor force constants in a rectangular (rather than square) lattice; (2) an ‘‘axially symmetric’’ model, which augments the model of Ref. [14] by incorporating bond-bending contributions to the force constants [34, 35]:

$$\Phi_{\alpha\beta}(l\kappa, l'\kappa') = \gamma(l\kappa, l'\kappa') \hat{\mathbf{e}}_\alpha \hat{\mathbf{e}}_\beta + \tilde{\gamma}(l\kappa, l', \kappa') (\delta_{\alpha\beta} - \hat{\mathbf{e}}_\alpha \hat{\mathbf{e}}_\beta), \tag{A2}$$

$\tilde{\gamma}(l\kappa, l', \kappa')$ being the transverse spring constants.

The generalization # 1 modifies the elements in Eq. (A1) and gives nonzero values to elements that were zero in Eq. (A1) (such as $D_{xy}(1,1)$). The generalization #2 also modifies the nonzero elements in Eq. (A1). In both of these generalized models, we have obtained the effective 2×2 dynamical matrices for long wavelength acoustic and optical phonons, thereafter verifying that those phonons have a vanishing helicity and Berry curvature. The underlying reason, as proven in the main text, is that the force constant models we have adopted for bare phonons obey Eq. (5).

Appendix B: Molecular Berry curvature for in-plane phonons in BaMn₂Sb₂

In the Born-Oppenheimer approximation, the electronic ground state can accumulate nontrivial geometric phase when the ionic configuration evolves. This electronic Berry phase with respect to the ions’ displacement is termed as molecular Berry phase and the corresponding Berry curvature is called the molecular Berry curvature [12, 36]. Here, we calculate the molecular Berry curvature (MBC) for the in-plane phonons of BaMn₂Sb₂ and show that it vanishes as long as the two valleys have energy gaps of opposite signs (even when \mathcal{T} symmetry is broken by an exchange field through the valley Zeeman splitting).

The MBC tensor elements at zero temperature can be written as [12]

$$G(\mathbf{q}) = \begin{pmatrix} G_{xx}(1,1) & G_{xy}(1,1) & G_{xx}(1,2) & G_{xy}(1,2) \\ G_{yx}(1,1) & G_{yy}(1,1) & G_{yx}(1,2) & G_{yy}(1,2) \\ G_{xx}(2,1) & G_{xy}(2,1) & G_{xx}(2,2) & G_{xy}(2,2) \\ G_{yx}(2,1) & G_{yy}(2,1) & G_{yx}(2,2) & G_{yy}(2,2) \end{pmatrix}, \tag{B1}$$

where

$$G_{\alpha\beta}(\kappa, \kappa'; \mathbf{q}) = \frac{i}{\mathcal{S}} \sum_{\mathbf{k}, s} \sum_{\substack{\epsilon_n < 0 \\ \epsilon_{n'} > 0}} \left[\frac{\langle \phi_{n,s}(\mathbf{k}) | \mathcal{M}_{\alpha}^{\kappa}(\mathbf{q}, s) | \phi_{n',s}(\mathbf{k} + \mathbf{q}) \rangle \langle \phi_{n',s}(\mathbf{k} + \mathbf{q}) | \mathcal{M}_{\beta}^{\kappa'}(-\mathbf{q}, s) | \phi_{n,s}(\mathbf{k}) \rangle}{(\epsilon_{n,s}(\mathbf{k}) - \epsilon_{n',s}(\mathbf{k} + \mathbf{q}))^2} - \frac{\langle \phi_{n,s}(\mathbf{k} + \mathbf{q}) | \mathcal{M}_{\beta}^{\kappa'}(-\mathbf{q}, s) | \phi_{n',s}(\mathbf{k}) \rangle \langle \phi_{n',s}(\mathbf{k}) | \mathcal{M}_{\alpha}^{\kappa}(\mathbf{q}, s) | \phi_{n,s}(\mathbf{k} + \mathbf{q}) \rangle}{(\epsilon_{n,s}(\mathbf{k} + \mathbf{q}) - \epsilon_{n',s}(\mathbf{k}))^2} \right], \quad (\text{B2})$$

\mathbf{q} is the phonon wave vector,

$$\mathcal{M}_{\alpha}^{\kappa}(-\mathbf{q}, s) = \sum_{\lambda} g^{\lambda,s}(\mathbf{q}) \frac{\partial u_{\mathbf{q}\lambda}}{\partial w_{\mathbf{q},\kappa,\alpha}} \quad (\text{B3})$$

is the electron-phonon interaction vertex for an electron in valley s when an atom κ undergoes a displacement $w_{\mathbf{q},\kappa,\alpha}$ along axis α , $|\phi_{n,s}(\mathbf{k})\rangle$ is the eigenstate of the free electron Hamiltonian (Eq. (2)) in band n at wave vector \mathbf{k} and valley s , $\epsilon_{n,s}(\mathbf{k})$ is the corresponding energy eigenvalue, $\sum_{\mathbf{k}} \equiv \mathcal{S} \int d^2k / (2\pi)^2$ and \mathcal{S} is the surface area of the sample.

The derivative in Eq. (B3) can be calculated from the relation [23]

$$\mathbf{u}_{\mathbf{q}\lambda} = \frac{1}{2M} \sum_{\kappa} M_{\kappa} \mathbf{w}_{\mathbf{q},\kappa} \cdot \mathbf{p}_{\mathbf{q}\lambda,\kappa}^* e^{-i\phi_{\lambda}}, \quad (\text{B4})$$

where $\mathbf{p}_{\mathbf{q}\lambda,\kappa}$ is the polarization vector denoting the displacement of atom κ in normal mode (\mathbf{q}, λ) , ϕ_{λ} is a (for now arbitrary) phase factor that originates from the fact that the polarization vectors $\mathbf{p}_{\mathbf{q}\lambda,\eta}$ of a given mode (\mathbf{q}, λ) are defined modulo an κ -independent phase factor, M_{κ} is the mass of atom κ , $2M$ is the atomic mass in the unit cell of two Sb atoms,

$$\mathbf{w}_{\mathbf{q},\kappa} = \frac{1}{N} \sum_{\mathbf{l}} e^{-i\mathbf{q}\cdot\mathbf{l}} \mathbf{w}_{\mathbf{l},\kappa}, \quad (\text{B5})$$

N is the number of unit cells and $\mathbf{w}_{\mathbf{l},\kappa}$ is the displacement of atom κ in a unit cell of position \mathbf{l} . The hermiticity conditions $\mathbf{w}_{\mathbf{l},\kappa}^{\dagger} = \mathbf{w}_{\mathbf{l},\kappa}$ and $u_{\mathbf{q}\lambda}^{\dagger} = u_{-\mathbf{q}\lambda}$ impose

$$e^{i\phi_{\lambda}} \mathbf{p}_{\mathbf{q}\lambda,\kappa} = e^{-i\phi_{\lambda}} \mathbf{p}_{-\mathbf{q}\lambda,\kappa}^*. \quad (\text{B6})$$

In the main text, we have taken the polarization vector of the optical phonons to be real and even in \mathbf{q} , while those of acoustic phonons were real and odd in \mathbf{q} . Consequently, Eq. (B6) implies that $\phi_{\lambda} = 0$ for optical phonons and $\phi_{\lambda} = \pi/2$ for acoustic phonons (we could have equally well taken $\phi_{\lambda} = -\pi/2$).

With the preceding caveats, it follows that

$$\mathcal{M}_{\alpha}^{\kappa}(-\mathbf{q}, s) = \frac{1}{2} \sum_{\lambda} g^{\lambda,s}(\mathbf{q}) p_{\mathbf{q}\lambda,\kappa,\alpha}^* e^{-i\phi_{\lambda}}, \quad (\text{B7})$$

with $\mathcal{M}_{\alpha}^{\kappa}(\mathbf{q}, s) = \mathcal{M}_{\alpha}^{\kappa}(-\mathbf{q}, s)^{\dagger}$.

For long-wavelength phonons, we have

$$\begin{aligned} \mathcal{M}_{\alpha}^{\kappa}(\mathbf{q}, s) &= \frac{1}{2} (\delta_{\kappa,1} - \delta_{\kappa,2}) (g^{A1,s} \delta_{\alpha,x} + g^{B1,s} \delta_{\alpha,y}) \\ &+ \frac{i}{2} (\delta_{\kappa,1} + \delta_{\kappa,2}) [(g^{LA,s} \cos \chi + g^{TA,s} \sin \chi) \delta_{\alpha,x} + (g^{LA,s} \sin \chi - g^{TA,s} \cos \chi) \delta_{\alpha,y}], \end{aligned} \quad (\text{B8})$$

where δ_{ij} is Kronecker's delta, χ is the angle between $\hat{\mathbf{q}}$ and $\hat{\mathbf{x}}$, and the i in the second line comes from the fact that $\phi_{\lambda} = \pi/2$ for acoustic phonons. The first and second lines in Eq. (B8) originate from optical and acoustic phonons, respectively. The optical deformation potentials $g^{A1,s}$ and $g^{B1,s}$ are defined in Eq. (36). The acoustic deformation potentials $g^{LA,s}$ and $g^{TA,s}$ are defined in Eqs. (38) and (41).

Substituting Eq. (B8) in Eq. (B2), we compute the MBC explicitly. When \mathcal{T} -symmetry is present, Eq. (B2) vanishes identically due to perfect cancellation between the contributions from the two electronic valleys. Specifically, if we write

$$G_{\alpha\beta}(\kappa, \kappa'; \mathbf{q}) \equiv \sum_s G_{\alpha\beta}(\kappa, \kappa'; \mathbf{q}, s), \quad (\text{B9})$$

then we find $G_{\alpha\beta}(\kappa, \kappa'; \mathbf{q}, +) = -G_{\alpha\beta}(\kappa, \kappa'; \mathbf{q}, -)$ in the presence of \mathcal{T} -symmetry. It is nonetheless instructive to list the matrix elements of $G_{\alpha\beta}(\kappa, \kappa'; \mathbf{q}, s)$ to leading order in q :

$$\begin{aligned}
G_{xx}(1, 1; \mathbf{q}, s) &= -s \frac{i}{8\pi} \frac{\text{sign}(m_0)}{v^2} q g_z^o g_x^a \cos \chi \\
G_{yy}(1, 1; \mathbf{q}, s) &= -s \frac{i}{8\pi} \frac{\text{sign}(m_0)}{v^2} q g_x^o g_z^a \cos \chi \\
G_{xx}(2, 2; \mathbf{q}, s) &= -G_{xx}(1, 1; \mathbf{q}, s) \\
G_{yy}(2, 2; \mathbf{q}, s) &= -G_{yy}(1, 1; \mathbf{q}, s) \\
G_{xy}(1, 1; \mathbf{q}, s) &= s \frac{1}{16\pi} \frac{\text{sign}(m_0)}{v^2} (g_x^o g_z^o + i q (g_x^o g_z^a - g_x^a g_z^o) \sin \chi) \\
G_{yx}(1, 1; \mathbf{q}, s) &= -s \frac{1}{16\pi} \frac{\text{sign}(m_0)}{v^2} (g_x^o g_z^o - i q (g_x^o g_z^a - g_x^a g_z^o) \sin \chi) \\
G_{xx}(1, 2; \mathbf{q}, s) &= G_{xx}(2, 1; \mathbf{q}, s) = 0 \\
G_{xy}(1, 2; \mathbf{q}, s) &= s \frac{1}{16\pi} \frac{\text{sign}(m_0)}{v^2} (-g_x^o g_z^o - i q (g_x^o g_z^a + g_x^a g_z^o) \sin \chi) \\
G_{yx}(2, 1; \mathbf{q}, s) &= -s \frac{1}{16\pi} \frac{\text{sign}(m_0)}{v^2} (-g_x^o g_z^o + i q (g_x^o g_z^a + g_x^a g_z^o) \sin \chi) \\
G_{yx}(1, 2; \mathbf{q}, s) &= -G_{xy}(1, 2; \mathbf{q}, s) \\
G_{xy}(2, 1; \mathbf{q}, s) &= -G_{yx}(2, 1; \mathbf{q}, s) \\
G_{yy}(1, 2; \mathbf{q}, s) &= G_{yy}(2, 1; \mathbf{q}, s) = 0 \\
G_{xy}(2, 2; \mathbf{q}, s) &= -G_{yx}(1, 1; \mathbf{q}, s) \\
G_{yx}(2, 2; \mathbf{q}, s) &= -G_{xy}(1, 1; \mathbf{q}, s).
\end{aligned} \tag{B10}$$

We thus learn that all nonzero elements of $G_{\alpha\beta}(\kappa, \kappa'; \mathbf{q}, s)$ are proportional to the electronic valley Chern number, $\text{sign}(m_0)$. When the \mathcal{T} -symmetry is broken by an exchange field, the electronic bands undergo a Zeeman shift. As a consequence, the Dirac mass in both valleys will no longer have the same magnitude [37]. However, as seen from Eq. (B10), the MBC at each valley does not depend on the magnitude of the Dirac mass, but only on its sign. Hence, the total MBC vanishes even in the presence of a valley Zeeman splitting, provided that the later is not strong enough to induce a band inversion in one of the valleys.

Admittedly, a residual nonzero MBC could result from the \mathcal{T} -breaking perturbation, as the Dirac velocities as well as the strengths of the electron-phonon coupling in both valleys could be affected differently by B , thereby preventing a cancellation between valleys in the overall MBC. In that case, as per Eq. (B10), the resulting molecular Berry curvature would be proportional to the valley Chern number of electrons, this being a generalization of the result found by Saparov et al. in Ref. [12]. We have neglected this residual MBC in the treatment of Sec. VI.

-
- [1] L. Zhang, J. Ren, J.-S. Wang, and B. Li, Topological Nature of the Phonon Hall Effect, *Phys. Rev. Lett.* **105**, 225901 (2010).
 - [2] T. Qin, J. Zhou, and J. Shi, Berry curvature and the phonon hall effect, *Phys. Rev. B* **86**, 104305 (2012).
 - [3] Y. Liu, Y. Xu, and W. Duan, Berry phase and topological effects of phonons, *National Science Review* **5**, 314 (2017).
 - [4] Y. Liu, X. Chen, and Y. Xu, Topological phononics: From fundamental models to real materials, *Advanced Functional Materials* **30**, 1904784 (2020).
 - [5] Z.-K. Ding, Y.-J. Zeng, W. Liu, L.-M. Tang, and K.-Q. Chen, Topological phonons and thermoelectric conversion in crystalline materials, *Advanced Functional Materials* **34**, 2401684 (2024).
 - [6] Y. Jin, R. Wang, and H. Xu, Recipe for Dirac phonon states with a quantized valley Berry phase in two-dimensional hexagonal lattices, *Nano letters* **18**, 7755 (2018).
 - [7] S. Coh, Classification of materials with phonon angular momentum and microscopic origin of angular momentum, *Phys. Rev. B* **108**, 134307 (2023).
 - [8] Y. Xu, M. Vergniory, D.-S. Ma, J. L. Mañes, Z.-D. Song, B. A. Bernevig, N. Regnault, and L. Elcoro, Catalog of topological phonon materials, *Science* **384**, eadf8458 (2024).
 - [9] D. Xiao, M.-C. Chang, and Q. Niu, Berry phase effects on electronic properties, *Rev. Mod. Phys.* **82**, 1959 (2010).
 - [10] Y. Liu, Y. Xu, S.-C. Zhang, and W. Duan, Model for topological phononics and phonon diode, *Phys. Rev. B* **96**, 064106 (2017).
 - [11] T. Saito, K. Misaki, H. Ishizuka, and N. Nagaosa, Berry

- phase of phonons and thermal hall effect in nonmagnetic insulators, *Phys. Rev. Lett.* **123**, 255901 (2019).
- [12] D. Saporov, B. Xiong, Y. Ren, and Q. Niu, Lattice dynamics with molecular Berry curvature: Chiral optical phonons, *Phys. Rev. B* **105**, 064303 (2022).
- [13] J. Liu, J. Yu, J. L. Ning, H. Yi, L. Miao, L. Min, Y. Zhao, W. Ning, K. Lopez, Y. Zhu, *et al.*, Spin-valley locking and bulk quantum Hall effect in a noncentrosymmetric Dirac semimetal BaMnSb₂, *Nature communications* **12**, 4062 (2021).
- [14] L.-H. Hu, J. Yu, I. Garate, and C.-X. Liu, Phonon Helicity Induced by Electronic Berry Curvature in Dirac Materials, *Phys. Rev. Lett.* **127**, 125901 (2021).
- [15] M. Hamada, E. Minamitani, M. Hirayama, and S. Murakami, Phonon angular momentum induced by the temperature gradient, *Phys. Rev. Lett.* **121**, 175301 (2018).
- [16] H. Zhang, N. Peshcherenko, F. Yang, T. Ward, P. Raghuvanshi, L. Lindsay, C. Felser, Y. Zhang, J.-Q. Yan, and H. Miao, Observation of phonon angular momentum, arXiv preprint arXiv:2409.13462 (2024).
- [17] S. Parlak, S. Ghosh, and I. Garate, Detection of phonon helicity in nonchiral crystals with Raman scattering, *Phys. Rev. B* **107**, 104308 (2023).
- [18] K. H. Michel and B. Verberck, Phonon dispersions and piezoelectricity in bulk and multilayers of hexagonal boron nitride, *Phys. Rev. B* **83**, 115328 (2011).
- [19] A. A. MARADUDIN and S. H. VOSKO, Symmetry properties of the normal vibrations of a crystal, *Rev. Mod. Phys.* **40**, 1 (1968).
- [20] K. Sun, Z. Gao, and J.-S. Wang, Current-induced phonon Hall effect, *Phys. Rev. B* **102**, 134311 (2020).
- [21] We make the gauge choice to place the phase factor $\exp(\pm i\phi)$ always in front of $\sin(\theta/2)$. We could equally well have chosen to place the phase factors always in front of $\cos(\theta/2)$. Either choice will ensure that $|1\rangle\langle 2|$ has no discontinuities as the wave vector is varied ($|1\rangle\langle 1|$ and $|2\rangle\langle 2|$ already have that property irrespective of the gauge choice).
- [22] D. Sticlet, F. Piéchon, J.-N. Fuchs, P. Kalugin, and P. Simon, Geometrical engineering of a two-band Chern insulator in two dimensions with arbitrary topological index, *Phys. Rev. B* **85**, 165456 (2012).
- [23] P. Rinkel, P. L. S. Lopes, and I. Garate, Signatures of the Chiral Anomaly in Phonon Dynamics, *Phys. Rev. Lett.* **119**, 107401 (2017).
- [24] K. Saha, K. Légaré, and I. Garate, Detecting band inversions by measuring the environment: Fingerprints of electronic band topology in bulk phonon linewidths, *Phys. Rev. Lett.* **115**, 176405 (2015).
- [25] G. D. Mahan, *Many-particle physics* (Springer Science & Business Media, 2013).
- [26] P. Vogl, Microscopic theory of electron-phonon interaction in insulators or semiconductors, *Phys. Rev. B* **13**, 694 (1976).
- [27] K. Kaasbjerg, K. S. Thygesen, and K. W. Jacobsen, Phonon-limited mobility in *n*-type single-layer MoS₂ from first principles, *Phys. Rev. B* **85**, 115317 (2012).
- [28] Y. Song and H. Dery, Transport theory of monolayer transition-metal dichalcogenides through symmetry, *Phys. Rev. Lett.* **111**, 026601 (2013).
- [29] F. Giustino, Electron-phonon interactions from first principles, *Rev. Mod. Phys.* **89**, 015003 (2017).
- [30] K. Sun, Z. Gao, and J.-S. Wang, Phonon hall effect with first-principles calculations, *Phys. Rev. B* **103**, 214301 (2021).
- [31] L. Zhang, Berry curvature and various thermal hall effects, *New Journal of Physics* **18**, 103039 (2016).
- [32] X. Zhang, Y. Zhang, S. Okamoto, and D. Xiao, Thermal hall effect induced by magnon-phonon interactions, *Phys. Rev. Lett.* **123**, 167202 (2019).
- [33] I. Garate, Phonon-Induced Topological Transitions and Crossovers in Dirac Materials, *Phys. Rev. Lett.* **110**, 046402 (2013).
- [34] G. W. Lehman, T. Wolfram, and R. E. De Wames, Axially Symmetric Model for Lattice Dynamics of Metals with Application to Cu, Al, and ZrH₂, *Phys. Rev.* **128**, 1593 (1962).
- [35] L. Pintschovius, H. G. Smith, N. Wakabayashi, W. Reichardt, W. Weber, G. W. Webb, and Z. Fisk, Lattice dynamics of the A15 compound Nb₃Sb, *Phys. Rev. B* **28**, 5866 (1983).
- [36] C. A. Mead, The geometric phase in molecular systems, *Rev. Mod. Phys.* **64**, 51 (1992).
- [37] J. Qi, X. Li, Q. Niu, and J. Feng, Giant and tunable valley degeneracy splitting in MoTe₂, *Phys. Rev. B* **92**, 121403 (2015).